Bull Volcanol (2002) 64:117–133
DOI 10.1007/s00445-001-0188-8

RESEARCH ARTICLE

Rachel S. Hannah · Thomas A. Vogel · Lina C. Patino
Guillermo E. Alvarado · Wendy Pérez · Diane R. Smith

Origin of silicic volcanic rocks in Central Costa Rica: a study of a chemically variable ash-flow sheet in the Tiribí Tuff

Received: 12 September 2001 / Accepted: 30 October 2001 / Published online: 8 December 2001

Abstract Chemical heterogeneities of pumice clasts in an ash-flow sheet can be used to determine processes that occur in the magma chamber because they represent samples of magma that were erupted at the same time. The dominant ash-flow sheet in the Tiribí Tuff contains pumice clasts that range in composition from 55.1 to 69.2 wt% SiO_2. It covers about 820 km^2 and has a volume of about 25 km^3 dense-rock equivalent (DRE). Based on pumice clast compositions, the sheet can be divided into three distinct chemical groupings: a low-silica group (55.1–65.6 wt% SiO_2), a silicic group (66.2–69.2 wt% SiO_2), and a mingled group (58.6–67.7 wt% SiO_2; all compositions calculated 100% anhydrous). Major and trace element modeling indicates that the low-silica magma represents a mantle melt that has undergone fractional crystallization, creating a continuous range of silica content from 55.1–65.6 wt% SiO_2. Eu/Eu*, MREE, and HREE differences between the two groups are not consistent with crystal fractionation of the low-silica magma to produce the silicic magma. The low-silica group and the silicic group represent two distinct magmas, which did not evolve in the same magma chamber. We suggest that the silicic melts resulted from partial melting of relatively hot, evolved calc-alkaline rocks that were previously emplaced and ponded at the base of an over-thickened basaltic crust. The mingled group represents mingling of the two magmas shortly before eruption. Electronic supplementary material to this paper can be obtained by using the Springer LINK server located at http://dx.doi.org/10.1007/s00445-001-0188-8.

Keywords Arcs · Costa Rica · Magma batches · Partial melting · Silicic magmas

Editorial responsibility: T.H. Druitt
Electronic supplementary material to this paper can be obtained by using the Springer LINK server located at http://dx.doi.org/10.1007/s00445-001-0188-8.

R.S. Hannah · T.A. Vogel (✉) · L.C. Patino
Department of Geological Sciences, Michigan State University, East Lansing, MI 48824-1115, USA
e-mail: vogel@msu.edu
Tel.: +1-517-3539029, Fax: +1-517-3538787

G.E. Alvarado · W. Pérez
Escuala Centroamericana de Geología, Universidad de Costa Rica, Apdo. 35, San José, Costa Rica

D.R. Smith
Department of Geosciences, Trinity University, San Antonio, TX 78212-7200, USA

Introduction

This paper is part of a regional study of silicic volcanic deposits in Costa Rica. It addresses the problem of the origin of silicic magmas in arc settings, where continental crust is absent. In most of these arc settings, abundant silicic magmas are not common. In Costa Rica, the volcanic products are chemically bimodal. One population consists mainly of calc-alkaline basalts and andesitic flows with subordinate pyroclastic rocks. The other consists of voluminous silicic ash-flow sheets (ignimbrites) and air-fall deposits of dacitic to rhyolitic composition. Geochemical analyses of lavas and rare fallout deposits from the Quaternary Central American volcanic arc have been described in numerous review papers in the last two decades (cf. Kussmaul and Sprechmann 1982; Kussmaul 1988; Carr et al. 1990; Rose et al. 1999; Patino et al. 2000). However, we know little about the geochemistry and age of the ash-flow sheets (Pushkar and McBirney 1968; Hahn et al.1979; Drexler et al. 1980; Rose et al. 1981; Alvarado et al. 1992; Rose et al. 1999). Costa Rica is of particular importance because these ash-flow sheets represent an unusual abundance of silicic volcanism in a setting that contains no continental crust.

A widely accepted model for the origin of silicic magmas in calc-alkaline arc settings is fractional crystallization of basalt or basaltic andesite melts (for example, see: Sisson and Grove 1993; Feely and Davidson 1994; Brophy et al. 1999; Hildreth and Fierstein 2000). An alternate model to explain the origin of potassium-rich silicic magmas in evolved arcs is the partial melting of previously emplaced arc-related igneous rocks (Roberts and Clemens 1993).

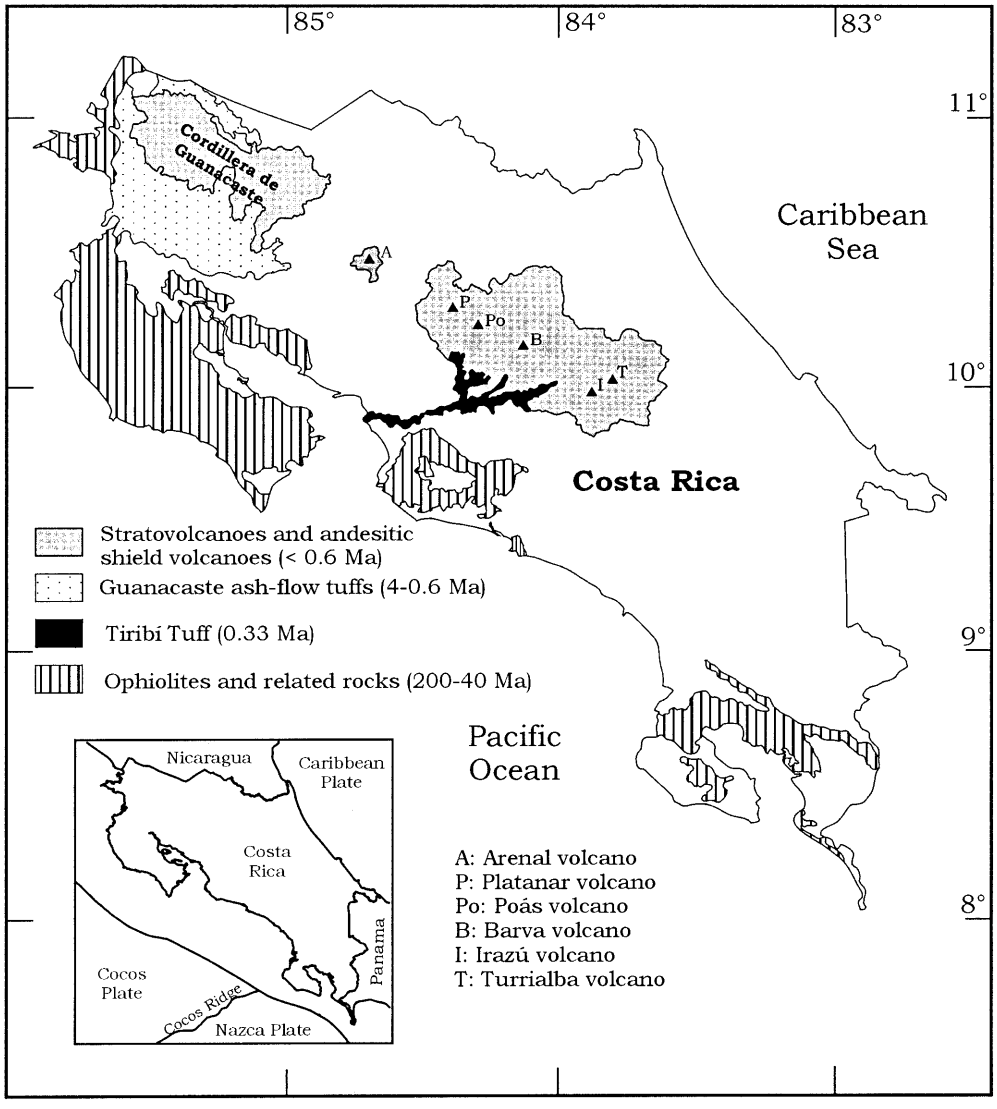

Fig. 1 Geologic map of Costa Rica showing stratovolcanoes and andesitic shield volcanoes of the modern arc, Guanacaste ash-flow tuffs, Tiribí Tuff, and ophiolites and related rocks. Also shown are the volcanoes in the Cordillera Central. Based on the map of Tournon and Alvarado (1997)

A major difficulty inherent to any fractional crystallization model in shallow reservoirs is the amount of fractionation required. Fractional crystallization of basaltic melts to produce high-silica melts would result in abundant cumulate rocks, which are not observed in these environments. In fact, in areas where the roots of silicic volcanic systems are exposed (for example, the Cordillera de Talamanca in southeastern Costa Rica, cumulate rocks are rare. Brophy et al. (1999) have recently suggested a model that may explain the scarce nature of the cumulate rocks and thus support the fractional crystallization model. They propose that the calc-alkaline series originated by fractionation near the crust–mantle boundary and, if this were the case, cumulate rocks would not be exposed. The base of the thickened Costa Rican crust could serve as an ideal density trap for magmas to pond.

The Tiribí Tuff in the Valley Central (Perez 2000; see below) is an example of silicic volcanism in Costa Rica (Figs. 1 and 2). It was selected for this study because it is a well-exposed, relatively large (see below) deposit that consists of two main ash-flow units (Perez 2000), and is chemically heterogeneous. Pumice clasts in the dominant, upper ash-flow sheet of this tuff belong to two distinct chemical groups (excluding mingled pumice clasts): one with 55.1–65.6 wt% SiO_2 and the other with 66.2–69.2 wt% SiO_2. The Tiribí Tuff, like all chemically heterogeneous ash-flow sheets, is ideal for evaluating magma evolution models because it represents instantaneous partial evacuation of the magma chamber. The chemical heterogeneities that were present in the magma body are preserved in the ash-flow sheet.

The origins of chemical heterogeneities in ash-flow sheets have been attributed to two major processes. The first, and widely accepted process involves large-scale differentiation of an originally homogeneous magma body (cf. Mittlefehltd and Miller 1983; Baker and McBirney 1985; McBirney and Nielson 1986; de Silva and Wolff 1995). The second involves discrete magma batches that are generated by partial melting and melt extraction, which are emplaced in a magma chamber. These processes were discussed by Marsh (1984), expanded upon by Bergantz (1989) and Sawyer (1994),

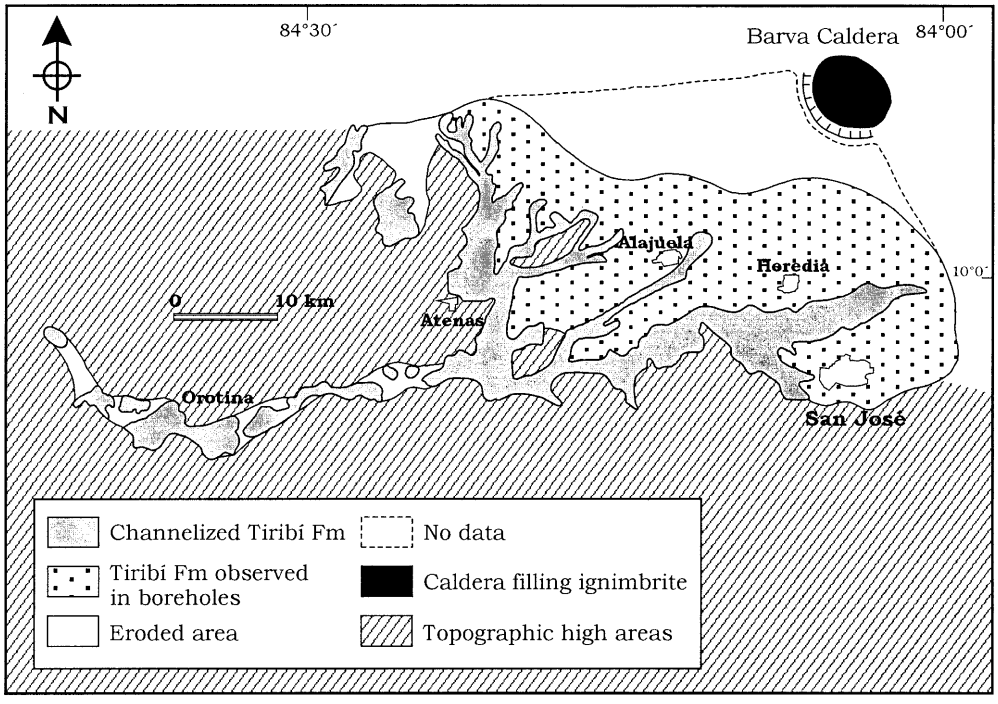

Fig. 2 Map showing the distribution of the Tiribí Tuff and the location of the Barva Caldera. Identified on the map is the Tiribí Tuff as river channel fill, and the ash-flow sheet based on drill cores. The topographic highs, where the Tiribí Tuff does not occur, are also shown

and amplified further by Eichelberger and co-workers (Eichelberger and Izbekov 2000; Eichelberger et al. 2000). There is petrologic evidence, reviewed in Mills et al. (1997) and Eichelberger et al. (2000), that many magma bodies may have had distinct compositional groups that cannot be related by crystal fractionation from a homogeneous magma body. Chemically distinct magma batches that are unrelated by fractionation can result from melting and extraction processes (Sawyer 1994). Crystal fractionation, assimilation, and magma mixing can subsequently modify these magma batches before they are emplaced in a high-level chamber.

Eichelberger et al. (2000) have suggested that many of these magma bodies were never stratified, but instead resulted from intrusion of a discrete magma body into another magma body. Eichelberger et al. (2000) have suggested two possible scenarios: the first is if a mafic magma intrudes a more silicic magma, an effusive eruption is common; the second is if a silicic magma intrudes a mafic magma body, a pyroclastic eruption is common. In the first scenario, the underplating of a silicic magma body by mafic magma has been widely documented (cf. Wiebe 1994; Coleman et al. 1995; Metcalf et al. 1995). In the second scenario, silicic magma is emplaced in a stored mafic body and, because of its buoyancy, rises rapidly through the mafic layer, retaining its integrity.

Workers have invoked models ranging from fractional crystallization of basaltic andesite to melting of previously emplaced island arc plutons to explain silicic rocks in an island-arc setting (cf. Roberts and Clemens 1993; Sisson and Grove 1993; Feely and Davidson 1994; Borg and Clynne 1998). We use these studies as a framework to evaluate the origin of the silicic and mafic magma compositions that occur in ash-flow sheets of the Tiribí Tuff of the Valle Central in Costa Rica.

Geological setting

The volcanic arc in Costa Rica developed as a result of subduction of the Cocos plate under the Caribbean plate (e.g., DeMets et al. 1990; Fig. 1). In Costa Rica, subduction-related volcanism has been present at least since the Upper Cretaceous, but more extensive volcanism developed between the Oligocene and Quaternary. Quaternary volcanic rocks are calc-alkaline (basalt to rhyolite trend) with some island-arc tholeiites (cf. Alvarado and Carr 1993; Tournon and Alvarado 1997). Alkaline volcanic rocks also occur, especially in the back arc (Tournon 1984).

Costa Rica is underlain by an over-thickened crust that is approximately 40 km thick (Sallarès et al. 2001a, 2001b). Recent studies suggest that the Costa Rican lithosphere represents an oceanic plateau (Bowland and Rosencrantz 1988; Gursky 1988; Donnelly 1994; Alvarado et al. 1997; Sinton et al. 1997; Christeson et al. 1999; Hauff et al. 2000). Hauff et al. (2000) concluded that this crust is part of the Caribbean Large Igneous Province, which has been involved with subduction-related volcanism in its western margin since the Middle to Late Cretaceous. Others have suggested that Costa Rica represents the remnant of a Jurassic island arc that originated independently of the Caribbean plateau and was accreted onto its western margin (Wildberg 1984; Frisch et al. 1992). However, recent $^{40}Ar/^{39}Ar$ results have cast doubts on this idea (Sinton et al. 1997). The origin of the Costa Rican crust is still a

matter of debate. However, regardless of its origin, this crust is not of continental origin; instead, it is composed of mafic meta-igneous rocks and some "anorthosite–gabbro" cumulates (Sachs and Alvarado 1996; Cigolini 1998).

The Tiribí Tuff outcrops mainly in the Valle Central, which is a volcanic–sedimentary basin between the Cordillera de Tilarán to the north and the Cordillera Central to the east, and along the Río Grande near the Pacific coast (Figs. 1 and 2). There are five large volcanoes in the Cordillera Central: Platanar (dormant), Poás (active), Barva (dormant), Irazú (active), and Turrialba (active). South of these volcanoes, the shallow subduction of the Cocos Ridge prevents further volcanism (Alvarado et al. 1992).

The Tiribí Tuff of Valle Central, Costa Rica

The Tiribí Tuff is dominated by ignimbrites and is one of the most important pyroclastic units in the central part of Costa Rica. Very little was known before 1999 about the stratigraphy, volcanology, and petrology of the Tiribí Tuff. Dengo and Chaverri (1951) and Williams (1952) published the first work describing the overall geology of the Valle Central, and they identified the pyroclastic origin of the rocks that are sandwiched between lava flows of the Colima and Barva Formations. In their distal parts, these rocks overlie Tertiary rocks. Previous workers used various terms for the gray tuff: "Glowing avalanche deposits" (Williams 1952), "Tiribí Formation" (Echandi 1981), and "Avalancha Ardiente Formation" (Kussmaul and Sprechmann 1982). In this paper we call this unit the Tiribí Tuff. This tuff can be traced from the foot of the volcanoes in the Cordillera Central to at least 75 km to the west near the Pacific coast (Fig. 2). In this transect, along the Río Grande near the Pacific coast, it was named Orotina Formation by Madrigal (1970). Perez (2000) described the stratigraphy, distribution, and source areas of these ignimbrites. She included the Orotina Formation, which was deposited in canyon and meandering channels, as part of the distal portion of the Tiribí Tuff. In addition, Marshall and Idleman (1999) and Gans (2000, personal communication) have dated the Tiribí Tuff in the Central Valley at 0.331±0.010 Ma and, at the Pacific, coast at 0.336±0.018 Ma, which are identical ages.

The Tiribí Tuff contains two ash-flow sheets. The lower sheet is exposed only in one quarry and in drill cores. It is separated from the upper sheet by a thin soil. Our study concentrates on the upper ash-flow sheet because it is well exposed and comprises the dominant volume of the Tiribí Tuff. At the base of the upper ash-flow sheet, there is a Plinian air-fall deposit, which is 0.5–3.0 m thick. The best exposures occur in several quarries, deep canyons, and in numerous boreholes. The total thickness of the upper ash-flow sheet reaches about 100 m (average of 30 m). The estimated volume and areal extent are 25 km^3 (DRE) and 820 km^2, respectively. The flow is divided into four main facies, based on the amount of welding, lithic and juvenile clast contents, fabric, and the size and presence of columnar jointing. The chemical variation of the juvenile clasts (pumice and fiamme) is the same in all the facies, which indicates to us a syn-eruption and co-magmatic origin for all facies. Based on isopach maps and stratigraphic correlations, Perez (2000) suggested that the different facies within the Tiribí Tuff erupted as multiple pulses in a short time (few years to thousands of years) from a composite caldera located in the Barva andesitic shield volcano (2,097 m above sea level).

The first chemical analyses of samples from the Tiribi tuff apparently were done by Schaufelberger and referred to in Dengo and Chaverri (1951).These analyses were limited to 21 samples (pumice samples in the tuff and the pumice-fall samples), which were dispersed over a large area. Previous workers (Williams 1952; Kussmaul and Sprechmann 1982; Tournon 1984; Kussmaul 1988; Appel 1990) described the general petrography, welding characteristics, color, and general geochemical trends (high-K andesites transitional to shoshonitic dacites) and compared these samples with those of the modern Costa Rican volcanoes. Our study includes 87 samples, which are glassy pumice samples from the ash-flow tuff. Samples are mostly from quarries and less commonly from road cuts.

Methods

Pumice clasts were sampled to represent the variation present within the dominant, upper ash-flow sheet of the Tiribí Tuff. Samples are glassy pumice clasts except for three samples of tuff. Three types of whole-rock chemical analyses were conducted: X-ray fluorescence (XRF), laser ablation inductively coupled plasma mass spectrometer analyses (LA-ICP-MS), and instrumental neutron activation (INAA). Major element and selected trace element concentrations were determined by XRF (Rigaku SMAX) for all samples. Trace element (including the rare earth elements) concentrations were also determined for selected samples by LA-ICP-MS (Cetac LSX-200 and Micromass Platform ICP-MS) and INAA. The two methods used for trace element analyses were compared by analyzing five samples by both INAA (University of Oregon) and LA-ICP-MS (Michigan State University) methods (Fig. 3). Nd and Sr isotopic analyses were made on four and ten samples, respectively, at Rutgers University.

Chemical analyses of phenocrysts were done by electron microprobe and LA-ICP-MS methods. The major element compositions of phenocrysts and glass matrix were determined by electron microprobe analyses (EMPA) at Indiana University. Trace elements (Ba, Sr, and Ca) of plagioclase phenocrysts and glass matrix were determined by LA-ICP-MS.

For whole-rock chemical analyses, samples were ground either with a ceramic flat plate grinder or in a

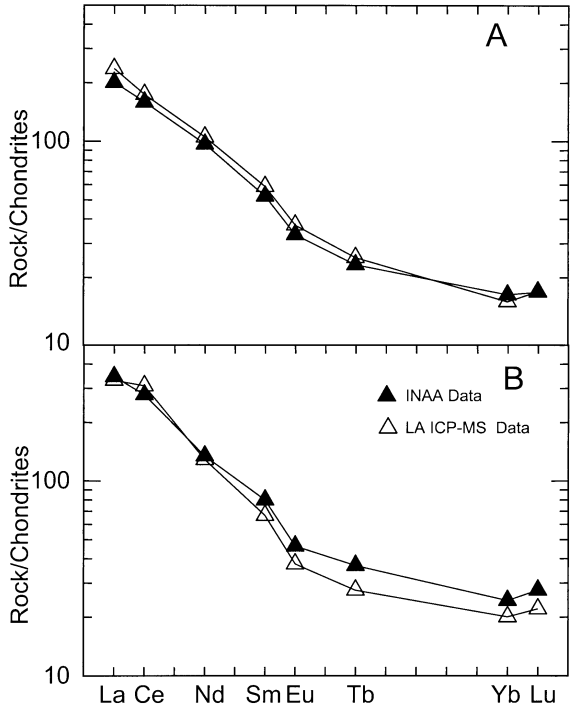

Fig. 3 Comparison of INAA and LA-ICP-MS for two samples. Five samples were analyzed by both techniques. The *upper diagram* represents the analyses of a single sample that were most similar; the *lower diagram* represents analyses of a single sample that showed the greatest differences

SPEX shatterbox with ceramic disk and puck, after passing them through a chipmunk. Two different techniques were used for preparation of glass disks: a high dilution fusion (HDF) and a low dilution fusion (LDF). The LDF glass disks were used for LA-ICP-MS. Glass disks were made by mixing the finely ground rock powder with lithium tetraborate as a flux and ammonium nitrate as an oxidizer. The proportion for HDF was 1 g rock, 9 g lithium tetraborate, and 0.25 g ammonium nitrate; for LDF these proportions were 3:9:0.50, respectively. These materials were mixed, fused at 1,000 °C in a platinum crucible in an oxidizing flame for at least 30 min, and then poured into platinum molds. The glass disks were analyzed by XRF and LA-ICP-MS.

XRF major element analyses were reduced by the fundamental parameter data reduction method (Criss 1980) using XRFWIN software (Omni Instruments). XRF trace element analyses were reduced by standard linear regression techniques. For LA-ICP-MS results, strontium was used as the internal standard (strontium concentration was determined by XRF on the same glass disks). Prior to calculation, the background signal was subtracted from standards and samples. The concentrations of the trace elements in the samples were calculated based on linear regression techniques using the BHVO-1, W-2, JB-2, JA-3, and BIR-1 standards. A comparison of INAA and LA-ICP-MS analyses of the same samples is shown in Fig. 3.

The glassy pumice clasts are secondarily hydrated, so the major elements are reported normalized to 100% anhydrous in the discussion and figures (data presented in Tables 1 and 2 are not normalized). Total Fe is reported as Fe_2O_3.

Petrography and phenocryst chemistry

Low-silica group

The low-silica group consists mainly of black and gray pumice clasts that are basaltic andesites. Crystal content varies in the low-silica group from crystal-rich (33% crystals) for samples with relatively low silica (about 56 wt% SiO_2), to crystal-poor (3% crystals) for samples with higher silica (about 62 wt% SiO_2; see below for discussion of chemical variation). The crystal-rich pumice contains 67% glass, 28% plagioclase ($An_{74–78}$), 4% clinopyroxene (Wo_{44} En_{47} Fs_9), and less than 1% olivine ($Fo_{70–73}$), with trace amounts of Fe-Ti oxides (magnetite and ilmenite), apatite, and rare amphibole. The crystal-poor pumice contains 97% glass, 2% plagioclase ($An_{35–58}$), and 1% clinopyroxene (Wo_{44} En_{47} Fs_9), with trace amounts of Fe–Ti oxides, apatite and rare amphibole. One xenocryst of plagioclase (An_{96}) was observed in the crystal-rich pumice. In the low-silica group, phenocrysts occur as isolated crystals and not as glomerophyric clots.

There are a variety of petrographic textures in the low-silica group. Plagioclase crystals range from euhedral crystals to anhedral crystals with highly irregular, cuspate boundaries. Many plagioclase phenocrysts have abundant melt inclusions, up to at least 50% glass inclusions, whereas other plagioclase phenocrysts have few or no melt inclusions. Pyroxene and olivine phenocrysts are euhedral. Olivine phenocrysts are often altered to iddingsite. Rare phenocrysts of amphibole are present. Vesicles within the glass of the low-silica group pumice clasts are well rounded.

Silicic group

The silicic group consists dominantly of light-colored (white or tan) pumice clasts that are crystal-poor dacites. They range in composition from 66.2 to 69.2 wt% SiO_2 (see below). Most samples are nearly aphyric, with 0–2% crystals by volume. In contrast to the low-silica group, phenocrysts occur as glomerophyric clots of plagioclase, clinopyroxene ($Wo_{42–47}$ $En_{45–47}$ $Fs_{8–12}$), orthopyroxene ($Wo_{3–6}$ $En_{69–75}$ $Fs_{22–29}$), and Fe–Ti oxides (dominantly magnetite, with minor ilmenite). Plagioclase compositions range from An_{34} to An_{49}. Alkali feldspar (sanidine) crystals (Ab_{48} Or_{43} An_8) occur, but are not common. Vesicles within the glass of the silicic group pumice clasts are generally tubular in shape.

Table 1 Selected glassy pumice samples from the Tiribí Formation. Major element oxides (wt%), other elements (ppm). *n.d.* Not determined

Sample	6-3:122197	13-2:122997	19-3:010498	1-5:121897	DEL2UC9[a]	990710-2	990713-4c
Location							
West	499.3	521.6	504.6	498.3	499.3	498.3	498.8
North	218.5	216.8	216.05	218.3	218.5	218.3	218.8
Pumice type	Low silica	Low silica	Low silica	Low silica	Low silica	Low silica	Low silica
XRF analyses							
SiO_2	53.80	54.80	58.66	61.50	62.16	62.37	62.62
TiO_2	0.88	0.93	1.01	1.05	1.21	1.15	1.08
Al_2O_3	19.60	19.70	18.43	16.30	16.23	16.15	15.67
Fe_2O_3	7.16	7.00	6.74	5.70	5.51	6.13	6.46
MnO	0.11	0.13	0.14	0.15	0.15	0.15	0.15
MgO	2.09	2.37	1.90	1.65	1.62	1.91	1.88
CaO	7.25	7.61	5.67	3.84	3.70	4.19	4.38
Na_2O	3.02	3.56	3.69	4.40	4.43	4.43	3.80
K_2O	2.28	2.38	2.86	3.77	3.61	3.54	3.39
P_2O_5	0.52	0.52	0.45	0.42	0.39	0.44	0.47
Total	96.71	99.00	99.55	98.78	99.01	100.46	99.90
Zn	84	76	74	84	87	86	94
Rb	55	61	78	101	94	88	90
Sr	867	918	685	595	573	602	637
Y	23	26	28	36	34	35	34
Zr	204	261	281	309	292	295	296
Nb	7	25	30	38	25	37	36
Ba	873	1,010	1,155	1,465	1,490	1,462	1,455
Laser ablation ICP-MS analyses							
La	n.d.	64.98	67.11	86.05	72.60	74.96	71.41
Ce	n.d.	113.33	124.83	158.08	148.00	136.13	139.33
Pr	n.d.	13.07	15.75	19.67	n.d.	17.15	17.75
Nd	n.d.	49.76	55.46	71.17	65.40	62.47	64.65
Sm	n.d.	8.95	9.62	12.27	11.30	11.58	11.92
Eu	n.d.	2.20	2.21	2.65	2.54	2.59	2.70
Tb	n.d.	1.00	1.08	1.28	1.20	1.24	1.21
Dy	n.d.	5.14	5.45	6.90	n.d.	6.58	6.44
Ho	n.d.	0.99	1.13	1.48	n.d.	1.23	1.24
Er	n.d.	2.83	3.17	3.88	n.d.	3.50	3.40
Yb	n.d.	2.49	2.85	3.69	3.78	3.40	3.44
Lu	n.d.	0.40	0.44	0.56	0.50	0.54	0.51
Hf	n.d.	5.44	6.54	9.10	8.20	7.80	7.35
Ta	n.d.	1.24	1.46	2.22	1.72	1.97	1.87
Pb	n.d.	6.69	6.12	11.33	0.00	8.23	8.54
Th	n.d.	14.05	17.20	22.13	17.50	20.36	18.75
U	n.d.	3.300	4.040	n.d.	n.d.	n.d.	n.d.
TIMS analyses							
$^{87}Sr/^{86}Sr$	0.703718	0.703724	n.d.	0.70373	n.d.	n.d.	n.d.
$^{143}Nd/^{144}Nd$	0.512951	0.512932	n.d.	0.51295	n.d.	n.d.	n.d.

[a] Trace elements analyzed by INAA

Banded pumice (mingled group)

Banded pumice clasts are transitional in composition between the low-silica and silicic groups (see below and Figs. 4, 5, and 6). Phenocrysts within the banded pumice are the same as those in the low-silica and silicic pumices. The banded pumice clasts are interpreted to be the result of mingling between the silicic and low-silica magmas. The proportion of light and dark bands reflects the whole-pumice composition; the greater the proportion of lighter bands, the higher the silica content (see below). Viscosity contrasts between the low-silica and silicic magmas most likely prevented mixing (Kouchi and Sunagawa 1983). Textural evidence for magma mingling includes flow banding of brown and white glass, reaction rims, and broken, rotated phenocrysts. Vesicles are often stretched in both dark and light bands.

Geochemistry

Major elements

Major element abundances for representative pumice clasts are listed in Tables 1 and 2. (A complete data set is available as electronic supplementary material at http://dx.doi.org/10.1007/s00445-001-0188-8). The pumice samples range from basaltic andesites and trachy-

Table 2 Selected glassy pumice samples from the Tiribí Formation. Major element oxides (wt%), other elements (ppm). *n.d.* Not determined

Sample	5-1:122097	990713-2f	2-1:121997	1-8:121897	1-3:121897	1-7:121897	DEL4C6[a]
Location							
West	515.85	498.8	527	498.3	498.3	498.3	498.3
North	217.1	218.8	216.9	218.3	218.3	218.3	218.3
Pumice Type	Mingled	Mingled	Silicic	Silicic	Silicic	Silicic	Silicic
XRF analyses							
SiO_2	57.80	61.88	63.11	64.40	65.90	66.20	68.08
TiO_2	1.00	1.16	1.05	0.74	0.75	0.74	0.70
Al_2O_3	17.90	15.99	16.99	15.60	15.60	15.50	15.42
Fe_2O_3	6.58	5.30	4.59	3.44	3.21	3.09	3.06
MnO	0.14	0.15	0.14	0.12	0.11	0.11	0.10
MgO	2.00	1.52	1.18	0.64	0.65	0.61	0.57
CaO	5.75	3.45	2.86	1.71	1.76	1.71	1.70
Na_2O	3.98	4.05	3.69	4.52	4.20	4.43	3.45
K_2O	3.03	3.90	4.10	5.34	5.25	5.32	5.18
P_2O_5	0.53	0.34	0.15	0.13	0.13	0.13	0.11
Total	98.71	97.74	97.86	96.64	97.56	97.84	98.37
Zn	79	85	84	70	66	67	49
Rb	78	97	112	140	137	135	127
Sr	761	541	507	280	294	273	266
Y	30	37	42	42	41	42	45
Zr	319	321	409	413	406	412	370
Nb	19	42	51	55	49	55	35
Ba	1,178	1,552	1,665	1,819	1,818	1,766	1,710
Laser ablation ICP-MS analyses							
La	74.45	73.41	84.58	78.19	78.43	76.99	82.00
Ce	131.03	143.31	174.84	189.13	191.54	186.29	165.00
Pr	17.05	17.24	17.73	18.73	19.17	18.34	n.d.
Nd	62.73	61.30	58.49	59.89	62.10	60.18	68.10
Sm	10.99	11.30	10.05	10.17	10.68	11.07	12.10
Eu	2.48	2.45	2.47	2.18	2.34	2.22	2.14
Tb	1.25	1.11	1.18	1.03	1.01	1.08	1.22
Dy	6.38	6.04	6.32	5.89	6.00	5.50	n.d.
Ho	1.35	1.18	1.40	1.29	1.28	1.25	n.d.
Er	3.73	3.15	3.82	3.33	3.35	3.07	n.d.
Yb	3.18	3.23	3.57	3.41	3.38	3.32	4.27
Lu	0.50	0.50	0.55	0.56	0.52	0.51	0.69
Hf	n.d.	7.58	8.65	8.95	8.12	9.29	10.70
Ta	n.d.	2.17	2.34	2.78	2.54	2.89	2.04
Pb	n.d.	9.51	14.98	24.87	18.76	25.58	
Th	n.d.	20.40	22.88	22.43	20.21	22.38	25.10
U	n.d.	n.d.	6.700	n.d.	n.d.	n.d.	n.d.
TIMS analyses							
$^{87}Sr/^{86}Sr$	n.d.	n.d.	n.d.	0.703733	0.703745	n.d.	n.d.
$^{143}Nd/^{144}Nd$	n.d.	n.d.	n.d.	0.512946	n.d.	n.d.	n.d.

[a] Trace elements analyzed by INAA

andesites to dacites, trachytes, and trachydacites (LeBas et al. 1986), with SiO_2 ranging from 55.1 to 69.2 wt% (anhydrous). They are enriched in potassium (Fig. 4), falling in both the high-K and shoshonitic fields.

Samples from the Tiribí Tuff fall into three compositional groups that, in general, correspond to the physical characteristics of pumice clasts (Fig. 4). The first group, the low-silica group, has silica ranging from 55.1 to 65.6 wt% and generally consists of black and gray pumice clasts (dark). The second group, the silicic group, has silica ranging from 66.2 to 69.2 wt% and generally consists of white and tan pumice clasts (light). The third group, the mingled group, has a composition that is intermediate between the low-silica group and the silicic group (silica ranges from 58.6 to 67.7 wt%). The mingled group includes only banded pumice clasts where distinct light and dark glass has been recognized either in hand samples or thin sections. Using these three general groupings, major element oxide trends are shown in Figs. 4 and 5. Based on point counting estimates of pumice types from quarries throughout the Tiribí Tuff, there is no systematic distribution of pumice types in the upper ash-flow sheet (Perez 2000).

There are many chemical differences between the silicic (white and tan pumice clasts) and the low-silica (black and gray pumice clasts) groups. First, samples from the low-silica group exhibit a large range in silica, from 55.1 to 65.6 wt% (Figs. 4 and 5). In general, the

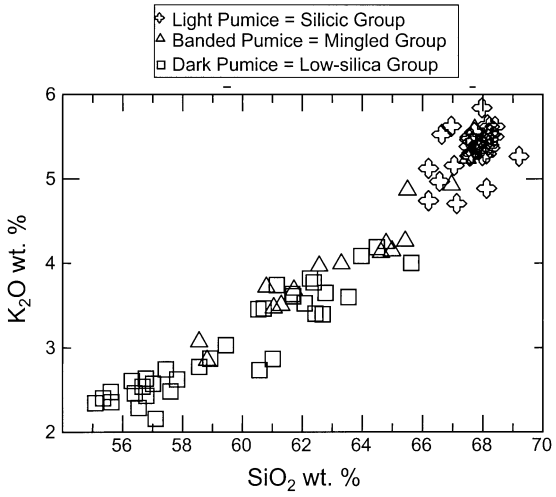

Fig. 4 K_2O versus SiO_2 variation for glassy pumice from the Tiribí Tuff. Samples are grouped according to whether they are dark (*squares*) or light colored (*crosses*), or if mingled (*triangles*) based on observed banding. All samples are from the upper ash-flow sheet, which comprises the dominant volume of the Tiribí Tuff

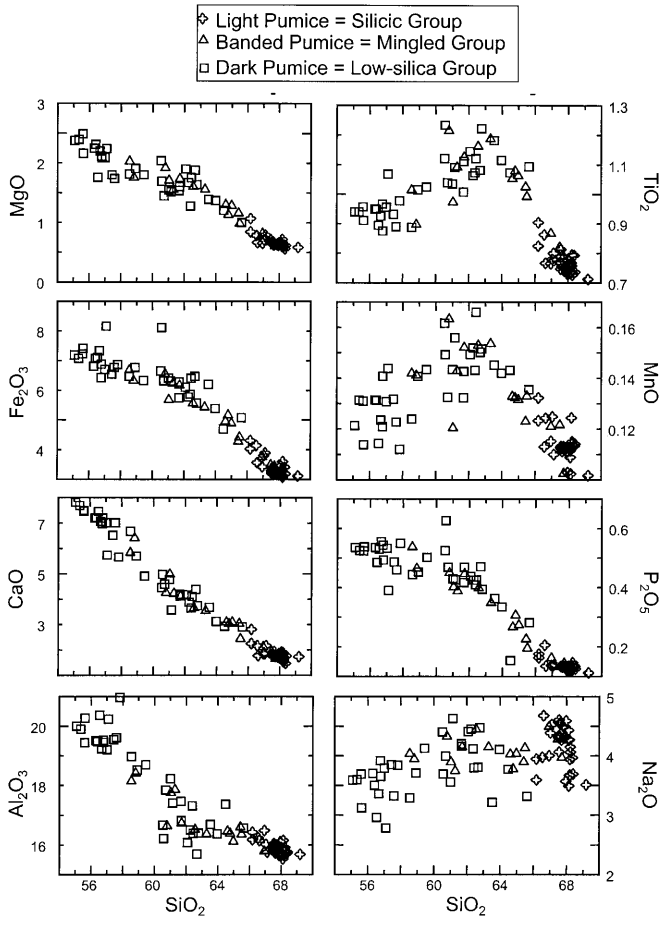

Fig. 5 Major element oxide variation plots versus SiO_2 for the Tiribí Tuff

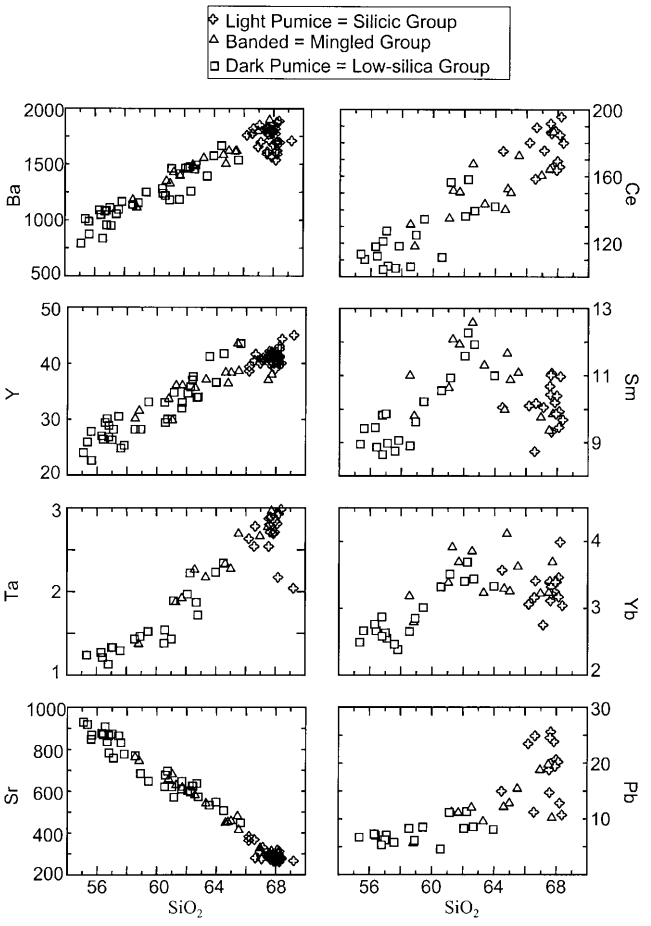

Fig. 6 Trace element variation plots versus SiO_2 for the Tiribí Tuff

major element oxides for the low-silica group have a linear relationship with silica. In contrast, samples from silicic group exhibit a small range in silica from 66.2 to 69.2 wt%. In the low-silica group, TiO_2 and MnO increase with increasing silica content, whereas in the silicic group, these oxides decrease with increasing silica content (Fig. 5).

Trace elements

Trace element abundances for representative pumice clasts are listed in Tables 1 and 2, and variations for some elements are illustrated in Fig. 6. (A complete data set is available as electronic supplementary material at http://dx.doi.org/10.1007/s00445-001-0188-8). Most trace elements show a linear relationship with silica content. However, the middle rare earth elements (MREE) and heavy rare earth elements (HREE) do not (e.g., Sm and Yb in Fig. 6).

Figure 7 depicts spider diagrams (normalized to primitive mantle concentrations) of Tiribí Tuff pumice clasts that represent the silicic group, low-silica group, and mingled group. The overall composition of Tiribí Tuff samples is consistent with magmas related to subduction

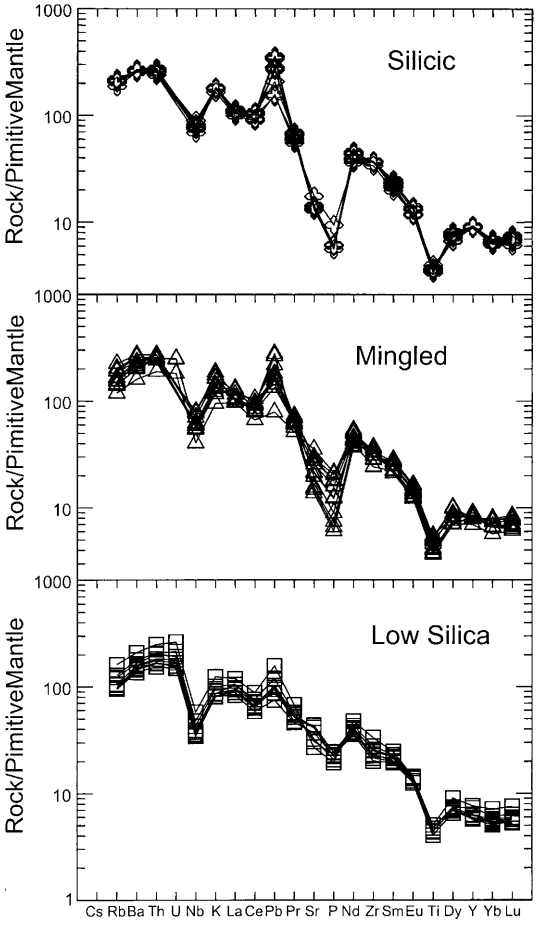

Fig. 7 Spider diagrams of representative pumice clasts from the low-silica, mingled, and silicic groups. Note that the silicic group has a much stronger depletion in P, and is enriched in the large ion lithophiles (Rb, Ba, K) in comparison to the low-silica group. Primitive mantle values from Sun and McDonough (1989)

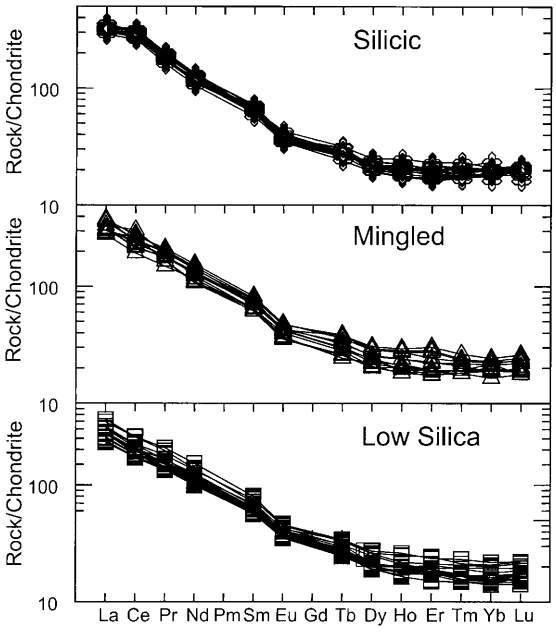

Fig. 8 Rare earth element plot for representative samples from the low-silica, silicic, and the mingled groups. The REE patterns for all samples within the Tiribí Tuff are very well constrained, with small degrees of variation. Chondrite values from Sun and McDonough (1989)

zone environments: enrichment in the large ion lithophile (LIL) and depletion in the high field strength (HFS) elements (e.g., Arculus 1994). The rare earth element (REE) patterns for all groups show a steep enriched pattern for light REE (LREE) and MREE with a flat HREE pattern (Fig. 8).

Laser ablation ICP-MS analyses of plagioclase phenocrysts and glass matrix for Ba/Sr and Sr/Ca ratios were made in order to evaluate the relationship between the low-silica and silicic groups (Fig. 9). The mean Ba/Sr ratio in the glass matrix from the low-silica group is 3.3 (SD=0.25), whereas the mean Ba/Sr ratio in glass from the silicic group is 13.0 (SD=1.14). The plagioclase phenocrysts from the two groups also have different Ba/Sr ratios, even though the major element compositions of the phenocrysts overlap ($An_{34–60}$). The Ba/Sr ratio of cores and edges of plagioclase phenocrysts from the low-silica group were compared with those from the silicic group. The Ba/Sr ratios for plagioclase phenocrysts in the silicic and low-silica pumice clasts are clearly different (Table 3, Fig. 9), showing no overlap even though both cores and rims are included. For example, none of the plagioclase cores in the silicic pumice clasts have the

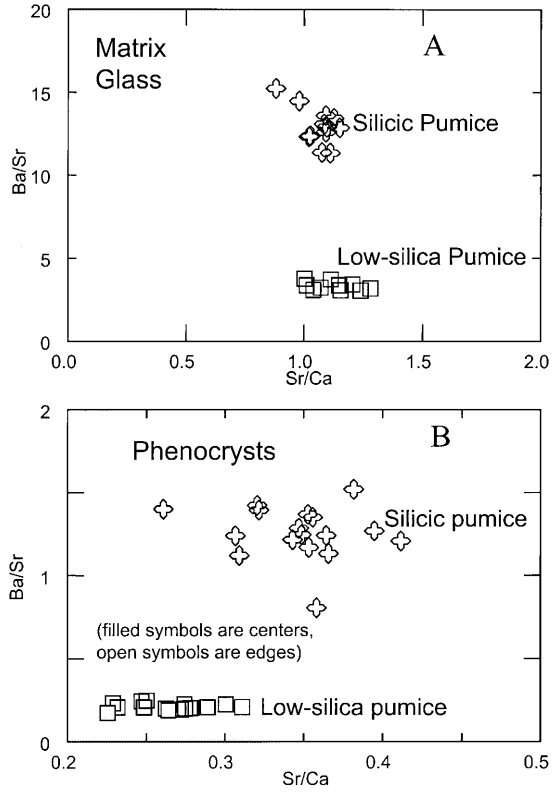

Fig. 9 Ba/Sr versus Sr/Ca for matrix glasses and plagioclase phenocrysts determined by LA-ICP-MS. *Upper diagram* is for glass from silicic and low-silica pumice samples. *Lower diagram* is for plagioclase grains from these pumice samples. *Filled symbols* are from the centers of plagioclase grains. *Open symbols* are from edges of plagioclase grains. Spot size of laser is about 25 µm. Note the distinct difference between the silicic and low-silica samples and that there is no evidence of plagioclase from the low-silica samples in the silicic samples

Table 3 ICP-MS laser ablation data for plagioclase phenocryst in high- and low-silica pumice

Variable	Pumice type	*n*	Mean	Median	SD	Minimum	Maximum
Ba/Sr	Silicic	17	1.257	1.244	0.160	0.806	1.520
Ba/Sr	Low silica	17	0.208	0.205	0.019	0.173	0.247
Sr/Ca	Silicic	17	0.347	0.353	0.036	0.261	0.411
Sr/Ca	Low silica	17	0.265	0.270	0.024	0.225	0.311

same composition as the plagioclase cores (or rims) from the low-silica pumice clasts. The mean of the Ba/Sr ratio of plagioclase from the low-silica group is 0.21 (SD=0.02), whereas the mean from the silicic group is 1.26 (SD=0.16). The fact that these data fall into two discrete populations (with no overlap) indicates to us that these phenocrysts originated from separate magma batches and that the silicic magma was not derived by the fractionation of the low-silica magma. The distinct ratios of the glasses (Fig. 9) also support this view.

Sr and Nd isotopes

Strontium and neodymium isotopes were analyzed in a VG Sector thermal ionization mass spectrometer at Rutgers University. Sr and Nd isotope ratios are reported as measured and normalized to $^{86}Sr/^{88}Sr$ of 0.1194 for Sr and $^{146}Nd/^{144}Nd$ of 0.7219 for Nd. $^{87}Sr/^{86}Sr$ and $^{143}Nd/^{144}Nd$ ratios for pumice samples from the silicic and low-silica groups are similar. For the low-silica group, $^{87}Sr/^{86}Sr$ values range from 0.703718 to 0.703734. For the silicic group, $^{87}Sr/^{86}Sr$ ratios range from 0.703705 to 0.703745. The $^{143}Nd/^{144}Nd$ isotope ratios from both groups also exhibit similar ranges, from 0.512932 to 0.512951.

Discussion

Origin of the low-silica group: crystal fractionation and magma chamber recharge

Within the low-silica group, trends in major element variation are consistent with magma evolution via crystal fractionation of a magma body (e.g., Gill 1981); MgO, Fe_2O_3, Al_2O_3, and CaO abundances decrease systematically as SiO_2 content increases, and K_2O and TiO_2 concentration increase (Figs. 4 and 5). The range of major and trace element compositions within the low-silica group can be modeled using batch fractional crystallization. These models were completed using multiple linear regression of major element oxides (Bryan et al. 1969; Wright and Doherty 1970; Table 4). Once the amount of each crystallizing phase was determined from the regression analysis, we predicted trace element concentrations for the daughter using a compilation of partition coefficients reported in Rollinson (1993).

For our models of crystal fractionation in the low-silica group, we assumed sample 13-2, with 55.75 wt% SiO_2 and 2.42 wt% K_2O (anhydrous values), to be the parental composition. Sample 13-2 is the most mafic sample for which we have microprobe data for the mineral phases. Table 4 lists modeling results for both major and trace elements, using steps A and B in Fig. 10A, where the sum of the squares of the residual ranges from

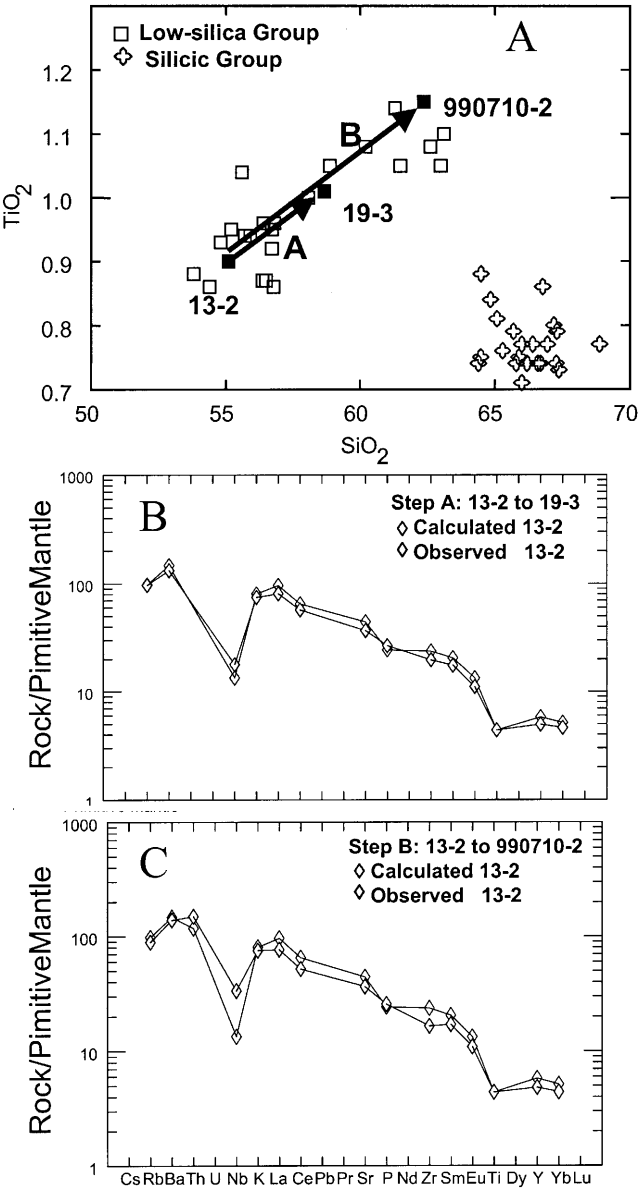

Fig. 10 **A** Multiple linear regression paths to evaluate fractional crystallization within the low-silica group. **B** and **C**. Spider diagram of observed and calculated (based on multiple linear regression) for steps A and B. In **B** and **C**, the data are normalized to the values of primitive mantle of Sun and McDonough (1989)

Table 4 Fractional crystallization models for the low-silica group

Step A				
Parent	13-2:122997			
Daughter	19-3:010498			
%	Min/rock			
18.3	Plagioclase			
1.8	Olivine			
1.5	Clinopyroxene			
1.1	Magnetite			
0.05	Apatite			
0.765	Liquid remaining			
Sum of the squares of the residual =0.091				
	Daughter	13-2; rock	13-2; Calc	Residual
SiO_2[a]	59.33	55.75	55.92	0.17
TiO_2	1.02	0.95	0.95	0
Al_2O_3	18.64	20.04	20.04	0
FeO	6.13	6.41	6.41	0
MnO	0.14	0.13	0.16	0.03
MgO	1.92	2.41	2.38	0.03
CaO	5.73	7.74	7.70	0.04
Na_2O	3.73	3.62	3.39	0.23
K_2O	2.89	2.42	2.25	0.17
P_2O_5	0.46	0.53	0.58	0.05
Prediction based on distribution coefficients				
Rb	79	62	61	1
Sr	692	934	774	160
Ba	1,168	1,028	924	103
Y	29	26	23	4
Zr	284	265	220	46
Nb	16	10	13	3
La	67.9	66.1	55.4	10.7
Ce	126.3	115.3	101.4	13.9
Sm	9.7	9.1	7.8	1.4
Eu	2.2	2.2	1.9	0.4
Yb	2.9	2.5	2.3	0.3
Step B				
Parent	13-2:122997			
Daughter	990710-2			
%	Min/rock			
31.7	Plagioclase			
3.1	Olivine			
2.3	Magnetite			
0.06	Apatite			
0.03	Clinopyroxene			
0.62	Liquid remaining			
Sum of the squares of the residual =0.03				
	Daughter	13-2; rock	13-2; Calc	Residual
SiO_2[a]	62.47	55.75	55.81	0.06
TiO_2	1.15	0.95	0.95	0
Al_2O_3	16.17	20.04	20	0.04
FeO	5.52	6.41	6.41	0
MnO	0.15	0.13	0.16	0.03
MgO	1.91	2.41	2.4	0.01
CaO	4.2	7.74	7.73	0.01
Na_2O	4.44	3.62	3.67	0.05
K_2O	3.55	2.42	2.26	0.16
P_2O_5	0.44	0.53	0.55	0.02
Prediction based on distribution coefficients				
Rb	88	62	56	6
Sr	603	934	767	167
Ba	1,465	1,028	968	60
Y	35	26	22	4
Zr	295	265	185	80
Nb	38	10	24	14
La	75.1	66.1	52.5	13.6
Ce	136.3	115.3	92.1	23.2
Sm	11.6	9.1	7.6	1.5
Eu	2.6	2.2	1.8	0.4
Yb	3.4	2.5	2.2	0.4

[a] In multiple linear regression calculations, all oxides are weighted as 1.0 except silica, which is 0.4

0.03 to 0.091 (which are well below acceptable values of Σr^2 by previous workers). Phases used in these models are those present in the most mafic pumice: plagioclase (An_{73}), olivine (Fo_{73}), clinopyroxene (Wo_{44} En_{47} Fs_9), magnetite, and apatite. The models can reproduce the chemical variation within the low-silica group with up to 38% crystal fractionation, with plagioclase as the dominant crystallizing phase. Batch fractional crystallization models based on the major elements reproduced the observed trace element concentrations as well. On average, the calculated concentrations are within 10% of the observed concentrations for trace elements (Fig. 10B, C).

While it is clear that fractional crystallization models can reproduce the chemical variation seen among low-silica group samples, the petrographic data provide evidence that other processes have occurred. For example, the existence of a plagioclase xenocryst (An_{96}) and heterogeneous plagioclase textures (abundant melt inclusions, no melt inclusions, partially resorbed, euhedral, etc.) within the same pumice fragment indicate to us that the low-silica magma was intruded or recharged by more primitive magma. Therefore, we suggest that the low-silica magma is the result of a combination of processes. Mafic magma representing a partial melt of the mantle and typical of island arc systems, intrudes into shallow levels beneath central Costa Rica. As this magma undergoes fractional crystallization, it is periodically recharged with fresh mafic magma, ripping up cumulates and introducing xenoliths to the system. Other workers have observed anorthitic xenoliths at Volcan Arenal and Volcan Poás in Costa Rica (Cigolini et al. 1991; Sachs and Alvarado 1996; Cigolini 1998) and interpreted them to represent products of magma recharge with erosion of cumulates in shallow-level magma chambers. This model can explain both the overall chemical trends seen in the Tiribí pumice clasts, and also the disequilibrium textures in some plagioclase phenocrysts. The systematic decrease in phenocryst content with increasing silica content in the low-silica samples is also consistent with a crystallizing and evolving magma body.

Origin of the silicic group: partial melting

The origin of silicic rocks within an island-arc environment has long been a controversy. In most island-arc settings, abundant silicic magmas are not common because of the absence of continental crust. In continental arcs, it is possible to assimilate or melt continental crust in order to achieve high proportions of silica in the melt. However, Costa Rica lacks a thick continental crust and this is not a plausible mechanism for producing the abundant silicic rocks that occur in that arc. There are two generally accepted models to explain the existence of silicic magmas in calc-alkaline island arcs. The first is fractional crystallization of basalt or basaltic andesite melts (Sisson and Grove 1993; Feely and Davidson 1994; Brophy et al. 1999). The second is partial melting of previously emplaced arc-related igneous rocks (Beard and Lofgren 1991; Roberts and Clemens 1993).

Previous studies have proposed a combination of convection-driven crystal fractionation, solidification fronts, and liquid segregation processes to explain the generation of silicic magmas from low-silica magmas (e.g., Marsh 1984; Brophy et al. 1999). In basaltic magma bodies, convection prevents large-scale crystal settling, which can drive magma chamber differentiation (Marsh 1984). Therefore, processes other than crystal settling have been proposed for magma differentiation. Brophy et al. (1999) proposed the following model. As fractional crystallization occurs, a solidification front descends downward into the magma body. At roughly 50% crystallization of a basaltic magma, convection above the solidification ceases, although convection still occurs below the solidification front. Above the solidification front, the crystal–liquid mush becomes rigid and can be fractured. If these fractures occur, they can drain evolved interstitial liquids out from the mush, which then migrate upwards by buoyancy-driven liquid/crystal segregation (Brophy et al. 1999). These evolved liquids represent a higher silica magma that is related to lower silica magma by fractional crystallization. These evolved liquids can accumulate in a magma chamber, which can be further fractionated by a similar process.

One of the problems of using fractional crystallization models to explain the origin of silicic magmas is the large amount of fractionation required to attain silicic compositions. The silicic magma of the Tiribí Tuff would require over 55% crystallization of plagioclase to evolve by fractional crystallization from the most mafic sample (13-2) to one of the most silicic samples (1-7). This fractionation would be dominated by plagioclase and would produce a significant increase in the Eu anomaly. If this process produced the magmas of the silicic group, they should have larger Eu anomalies than the presumed parental magmas of the low-silica group. However, for the Tiribí Tuff, this is not the case (Fig. 11A). Other rhyolites, in both continental and island arcs, have Eu anomalies that are pronounced, indicating large degrees of plagioclase fractionation (Brophy et al. 1999). In a plot of Eu/Eu* vs. SiO_2 (Fig. 11A), the distribution of the silicic and low-silica samples cannot be easily explained by fractional crystallization. If the silicic magmas were fractionating from low-silica magma, one would expect the linear trend of the low-silica group to continue into the silicic group without a break. Instead, the Eu/Eu* for the least silicic sample of the silicic group is higher (0.83) than the most silicic sample of the low-silica group (0.71; Fig. 11A).

The Ba/Sr and Sr/Ca ratios for plagioclase phenocrysts from the low-silica and silicic groups also can be used to argue against crystal fractionation. If fractionation of the low-silica magma were responsible for the origin of the silicic magma, one would expect that some plagioclase phenocrysts from the low-silica magma might be preserved as cores in the silicic magma. This is not the case (Table 3, Fig. 9). For these reasons, we re-

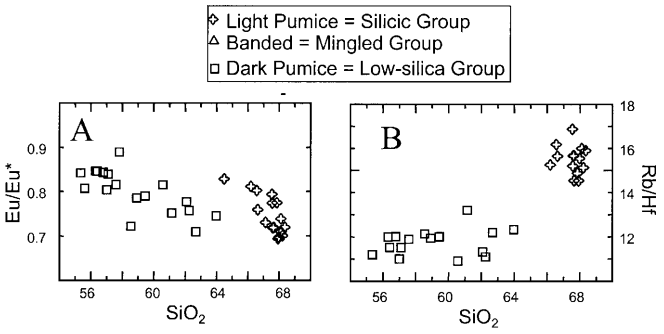

Fig. 11 **A** Plot of Eu/Eu* and **B** Rb/Hf versus SiO_2. Eu anomalies can be evaluated by calculating Eu* (Eu* can be calculated from the two linear equations $\log_{10}(Sm_N) = a*62+b$ and $\log_{10}(Tb_N) = a*65+b$) Eu/Eu* is a measure of the Eu anomaly. Note that the Eu/Eu* of the low-silica group and the silicic group are very similar. This would not occur if fractional crystallization of plagioclase were an important control on magma differentiation. Lines represent a multiple linear regression for each group. The Rb/Hf variation between the two groups indicates a different source for the silicic group

ject crystal fractionation as a major process in generating the silicic group magmas.

An alternative origin for the silicic magma is partial melting of a crustal source. Sr and Nd isotopes are commonly used to determine the source of magmas. However, if Sr and Nd isotopes are similar among different magma types, they could reflect either partial melting of the same source or partial melting of different sources that have similar ages. In the Tiribí Tuff, Sr and Nd isotopic ratios for both the silicic and low-silica magma batches are very similar. We interpret this to indicate that the low-silica and silicic group magmas originate from sources of similar ages. The isotopic data are not consistent with the partial melting of older oceanic crust for the origin of the silicic magma. However, the isotopic data are consistent with partial melting of younger, arc-related rocks. A further test for the petrogenesis of the silicic group is to evaluate Rb/Hf ratios. Crustal melts generally have higher Rb/Hf ratios than mantle melts. In Fig. 11B, the Rb/Hf ratios for the low-silica samples ranges from ~11 to 13, whereas the Rb/Hf ratios for the silicic group ranges from ~14.5 to 17. These ratios are consistent with the low-silica group, which represents mantle melts, and the silicic group, which represents melts derived from the lower crust (Geist et al. 1998; Price et al. 1999).

Incompatible trace element ratios can be used to monitor processes in magma bodies. If the variation in magma composition is caused by fractional crystallization, then the incompatible trace element ratio should show a regular variation with crystallization index. We have shown above that Rb/Hf ratios show two distinct groups among Tiribí samples. Similarly, Ba/Rb ratios are distinct for the low-silica and silicic magmas (Fig. 12A). In addition, the cumulative frequency distribution for the low-silica and silicic magmas occurs on two distinct trends, with the mingled samples occurring on an intermediate trend (Fig. 12B). A normal probability plot for

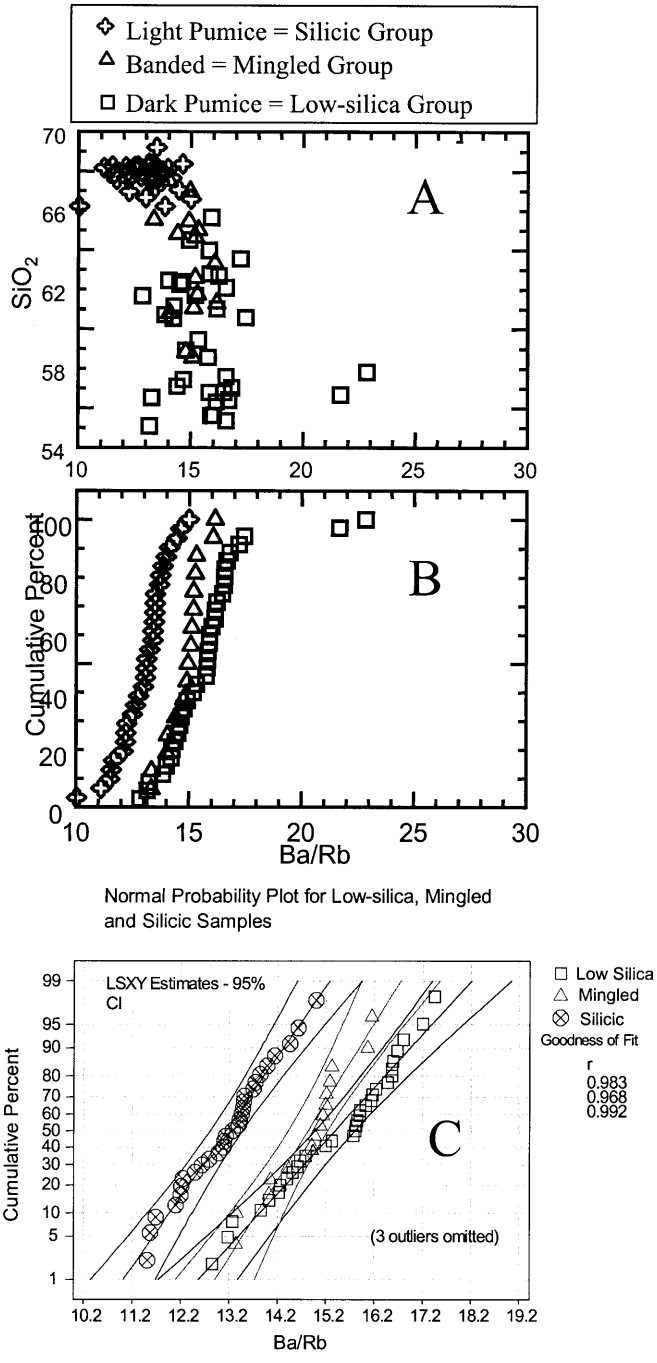

Fig. 12A–C Ba/Rb variation in glassy pumice from the Tiribí Tuff. **A** SiO_2 versus Ba/Rb. **B** Cumulative frequency distribution of Ba/Rb for the low-silica, silicic, and mingled pumice. Note how the distributions from the low-silica and silicic pumice samples fall on separate, unrelated curves. **C** Normal probability plot for the low-silica, silicic, and mingled pumice samples. Least squares linear distributions are shown for each pumice type with the 95% confidence limit (three outliers dropped). The *r*-values for the linear regression are shown

Ba/Rb ratios for the three types of samples (Fig. 12C) shows that each sample set defines a linear distribution with different slopes. This indicates different processes for each sample set.

A strong argument in favor of partial melting of different sources for the silicic and low-silica magmas is supported by concentrations of MREE within the silicic group. The LREE, such as La and Ce, behave incompatibly in both the low-silica and silicic groups (Fig. 6). The MREE and HREE elements, from Sm through Yb, behave differently in the low-silica and silicic groups. For example, in the low-silica group, Sm and Yb behave as incompatible elements that increase with silica content (Fig. 6). This is consistent with a magma that is undergoing fractional crystallization. However, these elements in the silicic group are depleted compared with the most silicic of the low-silica group samples, which indicates their behavior as compatible elements (Fig. 6). These data support our conclusion that the silicic group is not related to the low-silica group by fractionation processes, and further supports our proposal that the silicic magma was derived from a crustal source. One could argue that amphibole fractionation is causing enrichment in LREE and depletion in MREE. However, amphibole is extremely rare or absent in most samples.

Two partial melting processes may be responsible for the origin of the silicic group. First, the silicic group may represent the partial melt of a young, subducted slab. This is unlikely because yttrium concentrations in the silicic group are greater than 15 ppm (Fig. 6) and the Sr/Y ratios are less than 50 (Fig. 13), which are out of the range for adakitic rhyolites proposed to be slab melts (Defant and Drummond 1990). Second, the silicic group may represent a partial melt where hornblende and/or clinopyroxene were residual phases. Both clinopyroxene and hornblende as residual phases in the source would deplete the melt in MREE relative to LREE and HREE, which is observed in the silicic group. We recognize that crystal fractionation (perhaps accompanied by interaction with crustal rocks) could have played a minor role in the evolution of silicic magma, but argue that partial melting of crustal material is the dominant process that produced the geochemical characteristics observed in the silicic group. Melting of mafic sources yields melts with potash contents that are lower than those observed in the silicic group (Beard and Lofgren 1991). Melting of calc-alkaline granitoids can produce magmas with potash content similar to the silicic group (Skjerlie and Johnston 1993; Patiño Douce 1997), but these melts are more silicic than the silicic pumice clasts from the Tiribí Tuff (Smith et al. 1999). Unfortunately, no melt compositions are available for experiments that melt intermediate calc-alkaline rocks (Patiño Douce and McCarthy 1998; Patiño Douce 1999).

Magma mingling and mixing of low-silica and silicic magmas

The silicic and low-silica magmas erupted together to form the Tiribí Tuff. Textural evidence from banded pumice clasts indicates that there were two distinct magma batches that did not mix or equilibrate. Mingling of these magmas most likely occurred during evacuation of the magma chamber and resulted in banded pumice clasts.

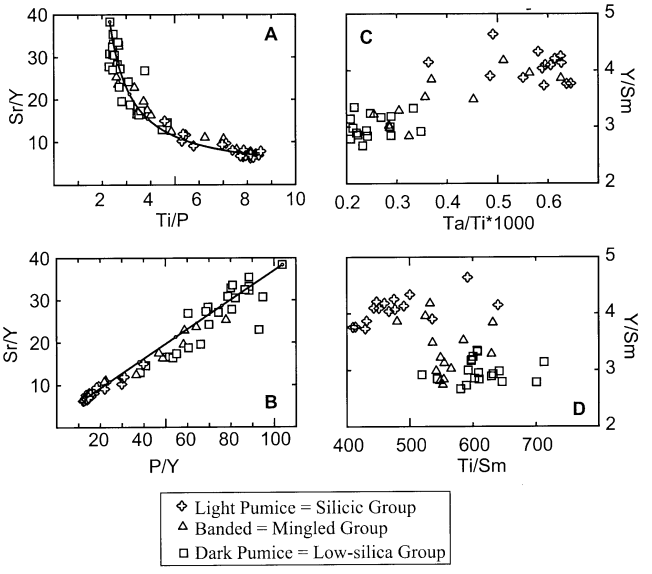

Fig. 13A–D Element ratio-ratio plots as a test for magma mixing/mingling. **A** and **C**. Plots of Sr/Y vs. Ti/P, and Y/Sm vs. Ta/Ti. In **A**, all the banded samples define a hyperbola, which supports mingling of the silicic and low-silica end members to form these compositions. In **B** and **D**, mixing is further tested by plotting the ratio of the denominators of the original ratio (P/Y) against one of the original ratios (Sr/Y), and Y/Sm versus Ti/Sm. The tick marks on the *hyperbola* (in **A**) and *line* (in **B**) represent 20% intervals. In **C** and **D**, the low-silica samples and silicic samples show nearly horizontal, separate trends, which indicates a non-mixing origin for the chemical variation within the low-silica and silicic groups. The banded pumice samples occur between the two end-member groups, confirming their mingled origin

The chemical variations within the mingled group are consistent with mixing. Mixing can be evaluated by using ratio–ratio plots of four separate elements: Sr, Y, Ti, and P (Fig. 13A), and Y, Sm, Ti, and Ta (Fig. 13C). If these ratios occur on a hyperbolic curve, a mixing process is supported (Fig. 13 A). A further test of mixing is a plot of the ratio of the denominators of the original ratio (e.g., P/Y) against one of the original ratios (e.g., Sr/Y; Fig. 13B). If the data for banded pumice clasts fall on a straight line, with the same two end members on the previous plot, then additional support for magma mixing or mingling is provided. These plots can also be used to test if the chemical variation of either the low or silicic magmas can be reproduced through homogeneous magma mixing. In similar plots (Fig. 13C, D) it is clear that, whereas the mingled pumice clasts fall on mixing lines between the two end members, the chemical variation within both the low-silica and the silicic group cannot be explained by magma mixing and that another process is necessary to explain the chemical variation within these groups. In addition, the trends of the MREE and HREE in the silicic group are also inconsistent with mixing within either the low-silica or the silicic groups.

Conclusions

The Tiribí Tuff contains three distinct groups of pumice clasts (the low-silica, silicic, and mingled groups), each requiring a different origin. The origin of the low-silica magma is consistent with fractional crystallization along with some magma recharge. Mafic magma originated by partial melting of metasomatized mantle and subsequently fractionated in the lower to middle crust to form the low-silica magma. While this magma underwent fractional crystallization, it was recharged by mafic magmas, which ripped up cumulates and mixed them back into the convecting magma chamber.

The silicic magma cannot be produced by fractional crystallization of the low-silica group magma. Based on Eu anomalies, MREE and LREE trends relative to silica, phenocryst chemistry, and frequency distributions of incompatible trace element ratios, the silicic magma is interpreted to have an origin independent of the low-silica magma. Ratios such as Ba/Rb, Ba/La, and Rb/Hf in the low-silica and silicic samples are consistent with different sources for those magmas. Ba/Sr ratios for cores and rims of plagioclase phenocrysts occurring in the low-silica and silicic magmas indicates that plagioclase from the low-silica magmas do not occur within the silicic samples, which also argues against a relationship between the two groups via fractionation. This interpretation is not unique to the Tiribí Tuff. There is petrologic evidence (reviewed in Mills et al. 1997; Eichelberger et al. 2000) that many magma bodies may have had distinct compositional groups that cannot be related to each other by fractionation processes alone.

Partial melting of previously emplaced, intermediate calc-alkaline rocks can produce the chemical composition of the silicic group, although the data required to verify this hypothesis have not been completed (Patiño Douce 1999). Because the Sr and Nd isotopes of the low-silica and silicic groups are similar, the ages of the sources for the two groups would have to be similar.

Our model is illustrated in a series of cartoons in Fig. 14. An episode of subduction zone magmatism resulted in intermediate calc-alkaline magmas, which ponded in or at the base of the thick Costa Rican crust. This was followed by passage and/or emplacement of new magma batches that heated the previously emplaced, still hot, calc-alkaline plutons, triggering partial melting that produced silicic magma. This silicic magma accumulated and migrated into the shallow crust, interacting with previously emplaced and evolving mafic magma(s). The emplacement of silicic magma into stored mafic magma resulted in the physical mixing of the magmas and eruption of the Tiribí Tuff. The cooler, silicic magma was emplaced in a crystallizing and hotter stored mafic body. Heating of the silicic magma by the hotter mafic magma prevented crystallization and resulted in nearly aphyric magma, whereas the more mafic magma was crystal rich. Both low-silica and silicic magmas were emplaced together; however, the silicic magma rose rapidly through the low-silica magma because of its negative buoyancy relative to the low-silica magma, retaining its integrity until it reached the fragmentation level (Eichelberger et al. 2000). Mingling between low-silica magma and silicic magma occurred at the boundaries between these magma types during eruption.

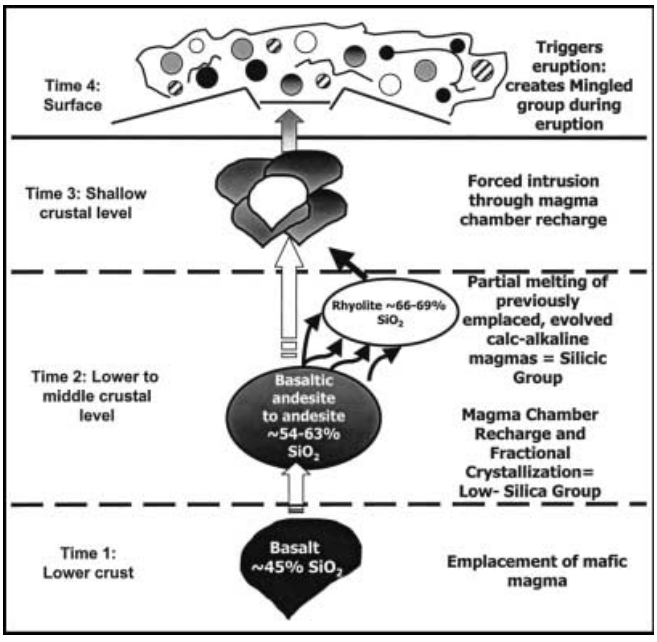

Fig. 14 Schematic model of the evolution of the Tiribí Tuff. *Time 1*, emplacement of subduction-related calc-alkaline, basaltic magma into the base of the over-thickened basaltic crust. This magma fractionates to andesitic magma. Some of this magma is emplaced to shallow, subvolcanic reservoirs, the remainder crystallizes into an intermediate composition pluton. *Time 2*, emplacement of new basaltic magma into the crystallized, but hot, intermediate pluton. Melting of the intermediate pluton occurs, resulting in a magma of silicic composition. *Time 3*, the silicic magma is emplaced through the shallow, subvolcanic magma reservoir, resulting in the eruption of the Tiribí Tuff

Acknowledgements This project was partially funded by a grant to R.S.H. for graduate research from GSA (Special A. Sesson Award for research in the Caribbean, GSA 6243-98) and by a grant to T.A.V. and L.C.P. from the National Science Foundation (NSF INT-9819236). D.R.S. thanks Thomas Gardner, Peter Sak, and Marino Protti for their insights into Costa Rican geology and assistance in the field, and also gratefully acknowledges Trinity University for financial support. Charles Bacon and Michael Dungan provided careful reviews that substantially improved the paper. We also thank Tim Druitt for his careful editing and patience.

References

Alvarado GE, Carr MJ (1993) The Platanar–Aguas Zarcas volcanic centers, Costa Rica; spatial-temporal association of Quaternary calc-alkaline and alkaline volcanism. Bull Volcanol 55(6):443–453

Alvarado GE, Kussmaul S, Chisea S, Guillot PY, Appel H, Wörner G, Rundle C (1992) Cuadro cronoestrátigrafico de las rocas ígneas de Costa Rica basado en dataciones radiométricas K–Ar y U–Th. J S Am Earth Sci 6(3):151–168

Alvarado GE, Denyer P, Sinton CW (1997) The 89 Ma Tortugal komatitic suite, Costa Rica: implications for a common origin of the Caribbean and eastern Pacific region from a mantle plume. Geology 25:439–442

Appel H (1990) Geochemie und K/Ar-Datierung on Magmatiten in Costa Rica Zentralamerika. MSc Thesis, Johannes Gutenberg Universitat Mainz

Arculus RJ (1994) Aspects of magma genesis in arcs. Lithos 33:189–208

Baker BH, McBirney AR (1985) Liquid fractionation Part III: geochemistry of zoned magmas and the compositional effects of liquid fractionation. J Volcanol Geotherm Res 24:55–81

Beard JS, Lofgren GE (1991) Dehydration melting and water-saturated melting of basaltic and andesitic greenstones and amphibolites at 1, 3, and 6.9 kb. J Petrol 32:365–401

Bergantz GW (1989) Underplating and partial melting: implications for melt generation and extraction. Science 245:1093–1095

Borg LE, Clynne MA (1998) The petrogenesis of felsic calc-alkaline magmas from the southernmost Cascades, California: origin by partial melting of basaltic lower crust. J Petrol 39:1197–1222

Bowland CL, Rosencrantz E (1988) Upper crustal structure of the western Colombian Basin, Caribbean Sea. Geol Soc Am Bull 100:534–546

Brophy JG, Whittington CS, Young-Rok P (1999) Sector-zoned augite megacrysts in Aleutian high alumina basalts: implications for the conditions of basalt crystallization and the generation of calc-alkaline series magmas. Contrib Mineral Petrol 135:277–290

Bryan WB, Finger LW, Chayes F (1969) Estimating proportions in petrographic mixing equations by least squares approximation. Science 163:926–927

Carr MJ, Feigenson MD, Bennett EA (1990) Incompatible element and isotopic evidence for tectonic control of source mixing and melt extraction along the Central American Arc. Contrib Mineral Petrol 105:369–380

Christeson GL, McIntosh KD, Shipley TH, Flueh ER, Goedde H (1999) Structure of the Costa Rica convergent margin, offshore Nicoya Peninsula. J Geophys Res 104:25443–25468

Cigolini C (1998) Intracrustal origin of Arenal basaltic andesite in the light of solid-melt interactions and related compositional buffering. J Volcanol Geotherm Res 86:277–310

Cigolini C, Kudo AM, Brookins DG, Ward D (1991) The petrology of Poas Volcano lavas; basalt–andesite relationship and their petrogenesis with the magmatic arc of Costa Rica. J Volcanol Geotherm Res 48:367–384

Coleman DS, Glazner AF, Miller JS, Bradord KJ, Frost TP, Joye JL, Bachl CA (1995) Exposure of a Late Cretaceous layered mafic–felsic magma system in the central Sierra Nevada batholith, California. Contrib Mineral Petrol 120:129–136

Criss JW (1980) Fundamental parameters calculations on a laboratory microcomputer. Advan X-ray Anal 23:93–97

Defant MJ, Drummond MS (1990) Derivation of some modern arc magmas by melting of young subducted lithosphere. Nature 347:662–665

DeMets C, Gordon RG, Argus DF, Stein S (1990) Current plate motions. Geophys J Int 101:425–478

Dengo G, Chaverris G (1951) Reseña geológica de la region sudoeste de la Meseta Central de Costa Rica. Revista Univ Costa Rica 5:313–326

de Silva SL, Wolff JA (1995) Zoned magma chambers: the influence of magma chamber geometry on sidewall convective fractionation. J Volcanol Geotherm Res 65:111–118

Donnelly TW (1994) The Caribbean Cretaceous basalt association: a vast igneous province that includes the Nicoya Complex of Costa Rica. Profil 7:17–45

Drexler JW, Rose WI, Sparks RSJ, Ledbetter MT (1980) Los Chocoyos Ash, Guatemala; a major stratigraphic marker in Middle America and in three ocean basins. Quat Res 13(3):327–345

Echandi E (1981) Unidades volcánicas de la vertiente norte de la cuenca de Río Virilla. Tesís Lic. Escuela de Geología – Universidad de Costa Rica, Costa Rica

Eichelberger JC, Izbekov P (2000) Eruption of andesite triggered by dike injection: contrasting cases at Karymsky Volcano, Kamchatka and Mount Katmai, Alaska. R Soc Lond Philos Trans A358:1465–1485

Eichelberger JC, Cherkoff, DG, Dreher ST, Nye CJ (2000) Magmas in Collision: Rethinking chemical zonation in silicic magmas. Geology 28:603–607

Feely TC, Davidson JP (1994) Petrology of calc-alkaline lavas at Volcan Ollague and the origin of compositional diversity at central Andean stratovolcanoes. J Petrol 35:1295–1340

Frisch W, Meschede M, Sick M (1992) Origin of the Central America ophiolites: evidence from paleomagnetic results. Geol Soc Am Bull 104:1301–1314

Geist D, Naumann T, Larson P (1998) Evolution of Galapagos magmas: mantle and crustal fractionation without assimilation. J Petrol 39:953–971

Gill J (1981) Orogenic andesites and plate tectonics. Springer, Berlin Heidelberg New York

Gursky HJ (1988) Gefüge, Zusammensetzung und Genese der Radiolarite im ophiolitischen Nicoya-Komplex (Costa Rica). Münstersche Forsch Geol Paläontol 68:1–89

Hahn GA, Rose W, Meyers T (1979) Geochemical correlation of genetically related rhyolitic ash-flow and air ashes, central and western Guatemala and the equatorial Pacific. Geol Soc Am Spec Pap 180:101–112

Hauff F, Hoernle K, van den Bogaard P, Alvarado G, Garbe-Schönberg D (2000) Age and geochemistry of basaltic complexes in western Costa Rica: contributions to the geotectonic evolution of Central America. Geochem Geophys Geosyst 1:1999GC000020

Hildreth W, Fierstein J (2000) Katmai volcanic cluster and the great eruption 1912. Geol Soc Am Bull 112(10):1594–1620

Kouchi A, Sunagawa I (1983) Mixing basaltic and dacitic magmas by forced convection. Nature 304:527–528

Kussmaul S (1988) Comparación petrológica entre el piso volcánico del Valle Central y la Cordillera Central de Costa Rica. Rev Cienc Technol 12(1–2):109–116

Kussmaul S, Sprechmann P, (1982) Estratigrafia de Costa Rica (America Central), II: Unidades litoestratigraficas igneas, vol 1. Actas 5 Congr Latinoameric Geol, Buenos Aires, pp 73–79

LeBas MJ, LeMaitre RW, Streckeisen A, Zanettin B (1986) A chemical classification of volcanic rocks based on the total alkali silica diagram. J Petrol 27:745–750

Madrigal R (1970) Geología del mapa básico Barranca, Costa Rica, Inf. Técn. y Not. Geol Año 9, no. 37. Dirección de Geol. Min. y Petrol. San José

Marsh BD (1984) Mechanics and energetics of magma formation and ascent. In: Boyd FR (ed) Studies in geophysics, explosive volcanism: inception, evolution and hazards. National Academy Press, Washington, DC, pp 67–83

Marshall JS, Idleman BD (1999) $^{40}Ar/^{39}Ar$ Age constraints on Quaternary landscape evolution of the Central Volcanic Arc and Orotina Debris Fan, Costa Rica. Geol Soc Am Meet 31:A479

McBirney AR, Nilson RH (1986) Reply to “Liquid collection in sidewall crystallization of magma: a comment on ‘liquid fractionation’” by S.A. Morse. J Volcanol Geotherm Res 30:163–168

Metcalf RV, Smith EI, Walker JD, Reed RC, Gonzales DA (1995) Isotopic disequilibrium among commingled hybrid magmas: evidence for a two-stage magma mixing-commingling process in the Mt. Perkins pluton, Arizona. J Geol 103:509–527

Mills JG Jr, Saltoun BJ, Vogel TA (1997) Magma batches in the Timber Mountain Magmatic System, Southwestern Nevada volcanic Field, Nevada, USA. J Volcanol Geotherm Res 178:185–208

Mittlefehltd D, Miller CF (1983) Geochemistry of the Sweetwater Wash Pluton, California; implications for “anomalous” trace element behavior during differentiation of felsic magmas. Geochim Cosmochim Acta 47:109–124

Patiño Douce AE (1997) Generation of metaluminous A-type granites by low-pressure melting of calc-alkaline granitoids. Geology 25:743–746

Patiño Douce AE (1999) What do experiments tell us about the relative contributions of crust and mantle to the origin of granitic magmas? Geol Soc Lond Spec Publ 168:55–75

Patiño Douce AE, McCarthy TC (1998) Melting of crustal rocks during continental collision and subduction. In: Hacker BR, Liou JG (eds) When continents collide: geodynamics and geochemistry of ultrahigh-pressure rocks. Kluwer, Boston, pp 27–55

Patino LC, Carr MJ, Feigenson MD (2000) Regional and local variations in Central American lavas controlled by variations in sediment input. Contrib Mineral Petrol 138:265–283

Perez W (2000) Vulcanologia y petroquimica del evento ignimbritico del Pleistoceno Superior (0.33 Ma) del Valle Central, Costa Rica. Escuela Centroamericana de Geologia, Universidad de Costa Rica

Price R, Stewart R, Woodhead J, Smith I (1999) Petrogenesis of high-K arc magmas: evidence from Egmont Volcano, North Island, New Zealand. J Petrol 40(1):167–197

Pushkar P, McBirney AR (1968) The isotopic composition of Sr in Central American ignimbrites. Annu Progr Rep no COO-689-92, Research Division of the US Atomic Energy Commission

Roberts MP, Clemens JD (1993) Origin of high-potassium calc-alkaline, I-type granitoids. Geology 21:825–828

Rollinson HR (1993) Using geochemical data: evaluation, presentation, interpretation. Longman, Essex, UK

Rose WI, Hahn GA, Drexler JW, Malinconico ML, Peterson PS, Wunderman RL (1981) Quaternary tephra of northern Central America. In: Self S, Sparks RSJ (eds) Tephra studies; proceedings of the NATO Advanced Study Institute “Tephra studies as a tool in Quaternary research” NATO advanced study institutes series. Ser C, Math Phys Sci 75:193–211

Rose WI, Conway FM, Pullinger CR, Deino A, MacIntosh WC (1999) An improved age framework for late Quaternary silicic eruptions in northern Central America. Bull Volcanol 61:106–120

Sachs PM, Alvarado GE (1996) Mafic metaigneous lower crust beneath Arenal Volcano (Costa Rica): evidence from xenoliths. Bol Observ Vulcanol Arenal 6(11–12):71–78

Sallarès V, Dañobeitia JJ, Flueh ER (2001a) Seismic tomography with local earthquakes in Costa Rica. Tectonophysics 329:61–78

Sallarès V, Dañobeitia JJ, Flueh ER (2001b) Lithospheric structure of the Costa Rican isthmus: effects of subduction zone magmatism on an oceanic plateau. J Geophys Res 106:621–643

Sawyer EW (1994) Melt segregation in the continental crust. Geology 22:1019–1022

Sinton CW, Duncan RA, Denyer P (1997) The Nicoya Peninsula, Costa Rica: a single suite of Caribbean oceanic plateau magmas. J Geophys Res 102:15507–15520

Sisson TW, Grove TL (1993) Experimental investigation of the role of H_2O in calc-alkaline differentiation and subduction zone magmatism. Contrib Mineral Petrol 113:143–166

Skjerlie KP, Johnston AD (1993) Fluid absent melting behavior of an F-rich tonalitic gneiss at mid-crustal pressure: implications for the generation of anorogenic granites. J Petrol 34:785–815

Smith DR, Noblett J, Reinhard AW, Unruh D, Chaberlain KR (1999) A review of the Pikes Peak batholith, Front Range, central Colorado: a “type example” of A-type granitic magmatism. Rocky Mt Geol 34:289–312

Sun S, McDonough WF (1989) Chemical and isotopic systematics of oceanic basalts: implications for mantle composition and processes. In: Saunders AD, Norry MJ (eds) Magmatism in the ocean basins. Geol Soc Spec Publ 42:313–345

Tournon J (1984) Magmatismes du Mesozoique à l'Actuel en Amérique Centrale: l'exemple de Costa Rica des ophiolites aux andésites. Thesis, Mémories Sciences Terre, Univ. Pierre et Marie Curie, Paris

Tournon J, Alvarado GE (1997) Carte géologique du Costa Rica: notice explicative: mapa geológico de Costa Rica: folleto explicativo, échele-escala 1:500, 000. Ed Tecnológica de Costa Rica, Mapa geológico de Costa Rica

Wiebe RA (1994) Silicic magma chambers as traps for basaltic magmas: the Cadillac Mountain intrusive complex, Mount Desert Island, Maine. J Geol 102:423–437

Wildberg H (1984) Die Nicoya-Komplex, Costa Rica. Zentralamerika: Magmaismus und Genese eines polygenetischen Ophiolith-Komplexes. Münstersche Forsch Geol Paläontol 62:1–123

Williams H (1952) Volcanic history of the Meseta Central occidental, Costa Rica. Univ Calif Publ Geol Sci 29:21–46

Wright TL, Doherty PC (1970) A linear programming and least squares computer method for solving petrologic mixing problems. Geol Soc Am Bull 81:1995–2000